

Extremely Nonlinear Optics Using Shaped Pulses Spectrally Broadened in an Argon- or Sulfur Hexafluoride-Filled Hollow-Core Fiber

Andreas Hoffmann ^{1,*}, Michael Zürch ^{1,†} and Christian Spielmann ^{1,2}

¹ Institute of Optics and Quantum Electronics, Abbe Center of Photonics, Friedrich-Schiller-University Jena, Max-Wien-Platz 1, 07743 Jena, Germany; E-Mails: michael.zuerch@uni-jena.de (M.Z.); christian.spielmann@uni-jena.de (C.S.)

² Helmholtz Institute Jena, Helmholtzweg 4, 07743 Jena, Germany

† Present address: Chemistry Department, University of California, Berkeley, CA 94720, USA

* Author to whom correspondence should be addressed; E-Mail: andreas.hoffmann.3@uni-jena.de; Tel.: +49-3641-9-47214; Fax: +49-3641-9-47232.

Academic Editor: Totaro Imasaka

Received: 23 September 2015 / Accepted: 16 November 2015 / Published: 20 November 2015

Abstract: In this contribution we present a comparison of the performance of spectrally broadened ultrashort pulses using a hollow-core fiber either filled with argon or sulfur hexafluoride (SF_6) for demanding pulse-shaping experiments. The benefits of both gases for pulse-shaping are studied in the highly nonlinear process of high-harmonic generation. In this setup, temporally shaping the driving laser pulse leads to spectrally shaping of the output extreme ultraviolet (XUV) spectrum, where total yield and spectral selectivity in the XUV are the targets of the optimization approach. The effect of using sulfur hexafluoride for pulse-shaping the XUV yield can be doubled compared to pulse compression and pulse-shaping using argon and the spectral range for selective optimization of a single harmonic can be extended. The obtained results are of interest for extending the range of ultrafast science applications drawing on tailored XUV fields.

Keywords: sulfur hexafluoride; nonlinear fiber optics; ultrashort laser pulses; pulse-shaping; atomic and molecular physics; high-harmonic generation

1. Introduction

During the past decades, high-harmonic generation (HHG) has been extensively studied to generate extreme ultraviolet (XUV) and soft-X-ray frequencies supporting the generation of pulses down in the attosecond range [1]. Additionally, the spectral, spatial and temporal properties of the HHG radiation make it a versatile tool in atomic and molecular spectroscopy [2]. To realize a matched source for the envisaged spectroscopic applications, much work has been done in controlling the shape of the HHG spectrum by either modifying the driving laser field [3,4] or using multicolor fields [5]. Using shaped driving laser fields is also a promising way to increase the HHG conversion efficiency. The high average power of optimized HHG sources allow now coherent diffraction imaging [6] which paves the way for using HHG sources for biological and medical applications [7], especially bearing in mind the ongoing effort to push HHG into the water window [8,9]. Two major scaling laws render HHG difficult for practical applications, namely:

(i) The cutoff law:

$$\hbar\omega_{\max} = I_p + 3.17 \cdot I \cdot \lambda^2 \quad (1)$$

It defines $\hbar\omega_{\max}$ the maximum photon energy of the XUV radiation which depends on the ionization potential of the atom or molecule I_p , the laser peak intensity I and λ the wavelength of the driving laser.

And (ii) the wavelength dependent conversion efficiency:

$$\eta(\lambda) \propto \lambda^{-6.5} \quad (2)$$

Taking Equations (1) and (2) into account for designing an HHG source it can be seen that, for a given laser intensity, the wavelength should be as long as possible to obtain the highest photon energy, which on the other hand results in a poor conversion efficiency. These two equations describing only single atom response already suggest the necessity to make a compromise. Optimization becomes even more important if collective effects are also considered. A higher laser intensity will not only give rise to higher photon energies, but also the conversion efficiency is reduced because almost all neutral atoms will be ionized before the intensity maximum is reached. Additionally, the freed electrons form a plasma which defocusses the laser and reduces the intensity further. The most important measure to avoid excessive ionization before the peak of the laser pulse is using driving pulses as short as possible [3]. The wavelength dependent conversion efficiency is also governed by phase-matching between XUV and driving laser pulse. The main sources of dephasing are the different index of refraction of the neutral gas, but also a major contribution stems from the dispersion of the generated plasma, the parameters of which strongly depend on shape, intensity and wavelength of the driving laser pulse [3]. So for almost all HHG optimization strategies it is beneficial to start with ultrashort laser pulses with controlled parameters.

One of the key techniques for controlling the shape and intensity of the driving laser pulses is spectral broadening in a noble gas-filled hollow-core fiber (HCF) and subsequent compression [10] and/or shaping [3]. For implementation of this scheme several optimizations of the setup can be done (Figure 1). Besides reduction of the inner diameter of the HCF to achieve the necessary intensities for self-phase modulation for laser systems with relatively low output peak powers, the design of the HCF

can be improved, e.g., hollow-core fiber photonic crystal fibers can lead to soliton self-compression [11]. To meet the desires for few-cycle pulse generation differential pumping schemes have been implemented to avoid ionization of the gas and accompanied coupling losses due to defocusing as well as higher order spectral phases which cannot be compensated appropriately by chirped mirrors [12]. A third way is to change the nonlinear medium, e.g., to a Raman-active molecular gas where the Raman activity allows spectral broadening beyond the scope of self-phase modulation.

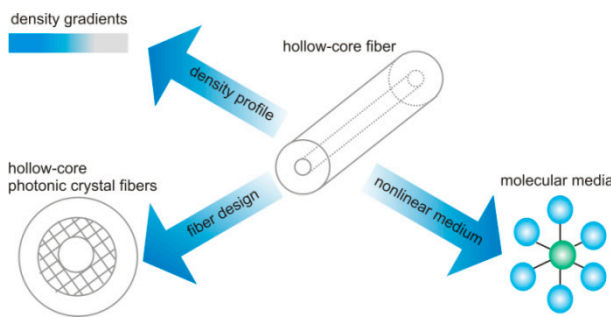


Figure 1. Improvement approaches for application of gas-filled hollow-core fibers for spectral broadening.

To enable highest degree of freedom in controlling the shape of the driving laser pulses, the fiber design, density profile and nonlinear medium have to be matched appropriately as shown in Figure 1. However, in this paper we limit ourselves to the investigation of the shaping capabilities using the molecular gas sulfur hexafluoride (SF_6) as the nonlinear medium. This molecule is a prominent example for ultrashort pulse generation via molecular phase modulation [13], dual-wavelength pumping [14,15], filamentation [16], generation of high-energy Raman-shifted Bessel beams [17] and spectral broadening and compression in hollow-core fibers [18].

In this paper we present the generation and shaping of HHG radiation using pulses which were spectrally broadened pulse in a gas-filled HCF and subsequently shaped with a phase only modulator. We will show that using SF_6 as nonlinear medium is advantageous compared to argon because it results in higher XUV yield and improved spectral selectivity. The paper is structured as follows: In Section 2 we describe the experimental setup, discuss the spectral broadening in an HCF for argon and SF_6 and the general scheme of pulse-shaping for HHG. The results of the pulse-shaping experiments are presented in Section 3. Conclusions and possible applications follow in Section 4.

2. Experimental Section

2.1. Experimental Setup

The experimental setup is shown in Figure 2. Ultrashort laser pulses from a regeneratively amplified titanium sapphire system (80 fs pulse duration, 0.9 mJ pulse energy, 1 kHz repetition rate) are spectrally broadened in a gas-filled hollow-core fiber (250 μm inner diameter, 0.8 m length, Hilgenberg, Malsfeld, Germany). Using a prism compressor with a deformable mirror as symmetry mirror Fourier-limited compression down to 20 fs can be achieved. However, here we put the focus on

the ability for shaping and optimizing the spectral phase. The shaped pulses are sent into a second argon-filled hollow-core fiber (HHG-HCF, Hilgenberg, Malsfeld, Germany, 140 μm inner diameter, 0.1 m length). This fiber is differentially pumped and used for high-harmonic generation in a 4-cm-long middle part of constant pressure. The generated XUV radiation is separated from the laser beam by an aluminum filter and is detected by a grazing-incidence XUV spectrometer (Jobin Yvon LHT 30 equipped with a PI-SX 400 back-illuminated XUV-CCD, Roper Scientific, Martinsried, Germany).

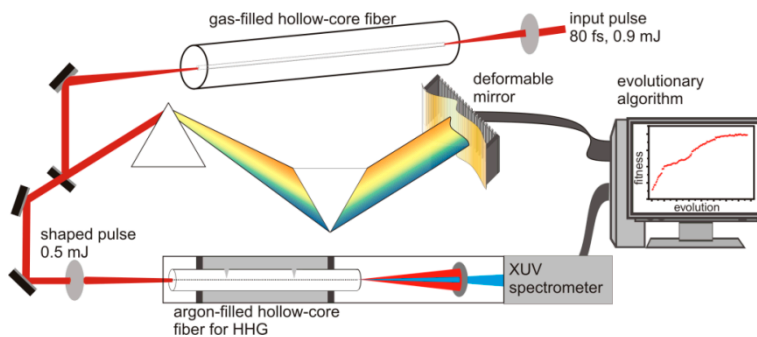


Figure 2. After spectral broadening in a gas-filled hollow-core fiber (HCF) laser pulses are sent through a prism-compressor with a computer-controlled deformable mirror for pulse shaping. Afterwards, the pulses are focused into an argon-filled capillary where they generate high harmonics. These are detected by an extreme ultraviolet (XUV) spectrometer and its signal is used as a feedback for an evolutionary algorithm.

Control over the high-harmonic spectrum is achieved by employing an evolutionary algorithm, which drives the gold membrane of the deformable mirror to shape the laser pulse. Deformation of the gold membrane depends on the voltage applied to electrodes behind the membrane (19 actuators, 0 to 300 V, 7 μm maximum deflection, $30 \times 8 \text{ mm}^2$ membrane surface) and changes the optical path of individual wavelength components and thus changes the spectral phase. With this setup it is possible to shape the high-harmonic spectrum by implementing different optimization goals [19].

2.2. Spectral Broadening in a Gas-Filled HCF

Spectral broadening in a gas-filled HCF is based on self-phase modulation (SPM) due to the intensity dependent refractive index $n(I)$ of the gas medium:

$$n(I) = n_0 + n_2 \cdot I \quad (3)$$

Here n_2 is the nonlinear refractive index, which is $1.6 \pm 0.3 \times 10^{-19} \text{ cm}^2 \cdot \text{W}^{-1}$ for SF₆ [20], being comparable to argon, but having a more complex behavior as is outlined as follows. SF₆ is a symmetric molecule and stretching vibrations have to be taken into account with particular importance on the A_{1g} vibrational mode being the strongest Raman active one. The fundamental frequency Ω_{Raman} of 775 cm^{-1} corresponds to a temporal period of 43 fs. For the presented experiments, the laser pulse duration is longer than the Raman oscillation period but shorter than the dephasing time T_2 of the stretching vibration, which is referred as transient or non-stationary scattering [21] and is limited by

$$1/\Omega_{\text{Raman}} < \tau_{\text{pulse}} \ll T_2 \quad (4)$$

T_2 is the inverse of the scattering bandwidth (6 ps for SF₆) [22]. Using fs pulses spectral broadening in SF₆ is governed by an interplay of SPM and stimulated Raman scattering (SRS), especially in an HCF where the intrinsic collinearity of the HCF avoids phase-matched SRS. SRS leads to sidebands in the spectrum at fixed positions (Figure 3b) in contrast to argon (Figure 3a), where only SPM is responsible for spectral broadening (experimental conditions as in Section 2.1.). Since achieving the same spectral broadening in SF₆ allows reduction of either the gas pressure or the input intensity compared to argon, it enables the transfer of this scheme to Yb based fiber lasers delivering rather long pulses [18].

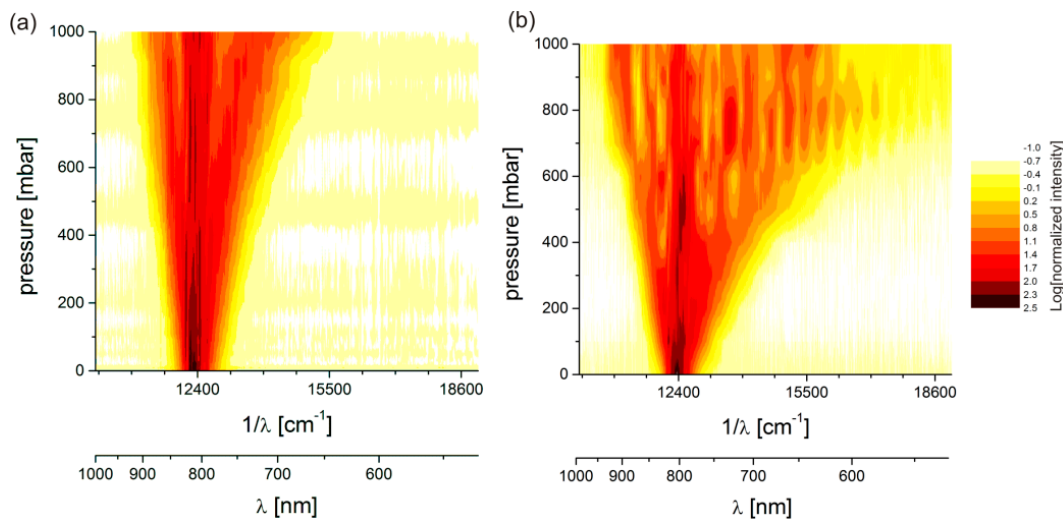


Figure 3. A comparison of spectral broadening in argon-filled (**a**) and SF₆-filled (**b**) HCF for different gas pressures shows possible benefits for pulse-shaping experiments. For SF₆ the spectral broadening is larger than for argon for otherwise comparable conditions. The generation of Raman sidebands is observed by vertical lines with higher amplitude at fixed positions which corresponds to the A_{1g} vibrational mode. Both figures show the spectral intensity in a joint logarithmic color scale which is normalized to the output pulse energy of the HCF.

For a better comparison of the applicability for pulse-shaping two broadened spectra (spectral range between 700 nm and 880 nm) and their corresponding Fourier transform assuming a flat spectral phase are shown in Figure 4. For SF₆ two observations should be pointed out: (i) the total spectral width is a few nanometers larger due to the enhanced redshifted part of the spectrum and (ii) the width of the central peak of the spectrum is larger due to the missing dip around 775 nm as for argon. Looking at the Fourier transform of both spectra there is not much difference in terms of pulse duration and shape. However, the presented pulse shaping scheme may benefit from the spectral characteristics of the SF₆-broadened spectrum due to the more favorable shape: (i) as a minor contribution the increase in total bandwidth directly translates into a better illumination of the deformable mirror surface and (ii) as a major contribution the spectral amplitude distribution is pronounced between 760 nm and 825 nm.

It should be emphasized that the pressure of SF₆ is chosen such that the SRS sidebands are weak and cannot be observed in Figure 4a. In this case the spectral phase is still smooth and pulse compression by prisms is possible [18]. However, the cross-phase modulation products of the

sidebands with the spectral distribution of the input pulse filling the spectral gaps compared to argon show clear evidence of Raman activity.

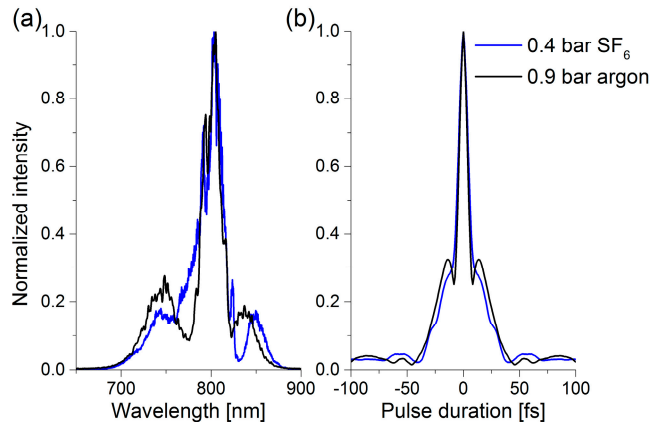


Figure 4. Spectrally broadened laser pulses after propagation through the hollow-core fiber (**a**) and their corresponding Fourier transform assuming a flat spectral phase (**b**) are compared for argon (black line) and SF₆ (blue line).

2.3. Tailored High-Harmonic Generation in a Gas-Filled HCF

A fair comparison of the advantages of pulses after spectral broadening in SF₆ and argon is very demanding and can be best judged in a subsequent highly nonlinear interaction experiment where it should become clear whether the additional contribution from SRS is beneficial or not. The spectral shape of the high-harmonic spectrum from a hollow-core fiber (Figure 5a) depends strongly on the evolution of the electric field of the driving laser pulse which can be controlled by shaping the spectral phase and amplitude. In the presented experiment the spectral phase is controlled with the pulse-shaper in order to reach the predefined optimization goal.

As outlined in the introduction the spectral shape of the HHG spectra depends on many parameters including single atom response and collective effects such as phase-matching. High-harmonic generation in a hollow-core fiber has additional phase-matching conditions (different fiber modes, increased interaction length) compared to a free-focus geometry offering optimization for enhancement or suppression of single harmonics (Figure 5c,d) besides optimization for total XUV yield (Figure 5b). For the HHG-HCF the total wavevector mismatch, which should be zero for maximum conversion efficiency, can be written as

$$\Delta k = (n(\omega_L) - n(m \cdot \omega_L)) \frac{\omega_L}{c} + \frac{\omega_p^2 \cdot (1 - m^2)}{2 \cdot m \cdot c \cdot \omega_L} + \frac{u_{nl}^2 \cdot c \cdot (1 - m^2)}{2 \cdot m \cdot a^2 \cdot \omega_L} \quad (5)$$

Here the three terms represent neutral gas dispersion (refractive index n , speed of light c), plasma dispersion (plasma frequency ω_p) and the geometric contribution from the hollow-core fiber (inner radius a , l -th root of the Bessel function $J_{n-1}(z)$ u_{nl}) for the m -th harmonic of the laser frequency ω_L [23]. Since the description of the propagation of the generating IR laser pulse and the harmonic radiation is full of twists and turns [24–26], *i.e.*, Equations (1) and (5) suggest a complex intensity and

wavelength dependence, the implementation of an evolutionary algorithm for finding the best suited pulse-shape is an established technique.

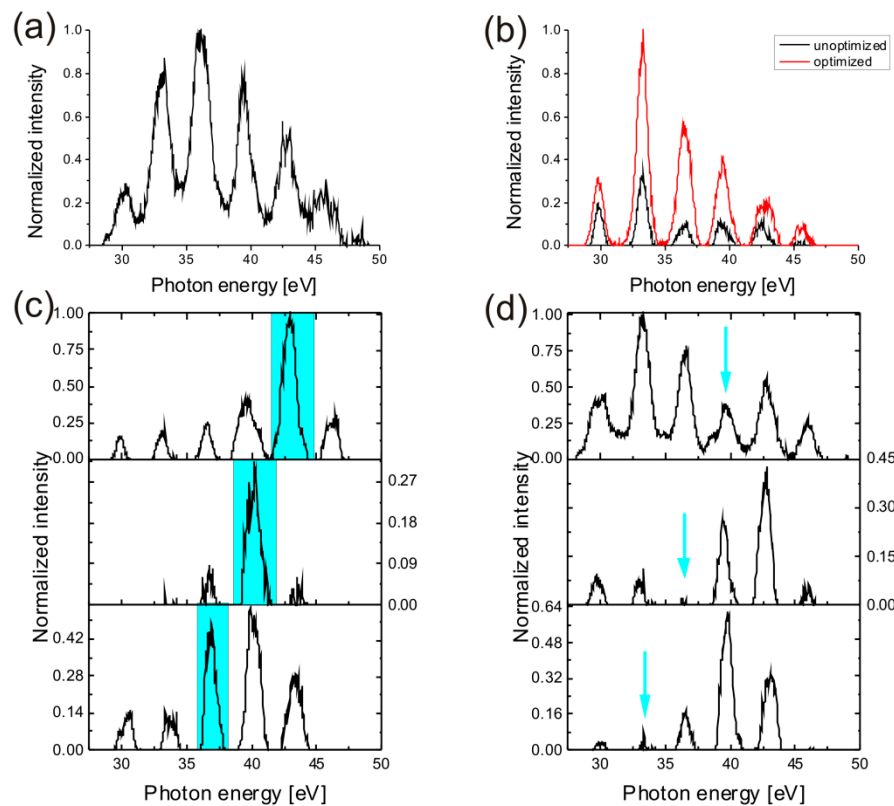


Figure 5. Different optimization goals for pulse-shaping experiments in HHG experiments. (a) is a typical HHG spectrum from a hollow-core fiber with a pulse that is compressed by translating the prisms for highest XUV yield and using a flat mirror surface; (b) shows an optimization of the overall yield by adaptively shaping the deformable mirror. By temporally shaping the driving laser pulse, a specified region of the spectrum (blue area) can be enhanced (c) or suppression of harmonics (blue arrows) can be achieved (d).

3. Results and Discussion

For comparison of the pulse-shaping capabilities of an argon and SF₆ spectrally broadened spectrum for generation of high-harmonics from a hollow-core fiber, two optimization scenarios are experimentally studied (pressure for both gases as in Figure 4): on the one hand, optimization of the total XUV yield and on the other hand selection of a single harmonic. For both experiments the conditions in the HHG-HCF are kept the same to ensure investigating only the influence of the slightly changed spectral shape for argon and SF₆ after broadening and the influence of the resulting temporal shaped laser pulses. For both experiments XUV spectra after optimization are shown as well as the development of the fitness parameter for the fittest individual of each generation. As parameters, 50 individuals per generation, a mutation rate of 0.5, a crossover rate of 0.4, a clone rate of 0.1 and 1500 ms acquisition time per individual were used.

3.1. Optimization of the XUV Yield

The optimization for the total XUV yield was performed for four different gas pressures in the HHG-HCF and the results are summarized in Figure 6, where the integrated signal between 23 nm and 43 nm was used as fitness parameter. At 10 mbar the obtained optimized HHG look very similar for the driving laser pulses broadened either in argon or SF₆. The 27th and 31st harmonics are slightly less pronounced, using SF₆ for broadening (Figure 6a). Inspecting the evolution of the fitness during the optimization as shown in the inset of Figure 6a it can be seen that the initial value for the fitness is much higher using SF₆, but the gradient is smaller. These observations are a first hint that the temporal shape of the SF₆-broadened pulse is slightly different. For 20 mbar backing pressure an increase for the 27th harmonic can be seen using SF₆. Since the gas pressure and the properties of the HHG-HCF are the same, this effect can only be attributed to plasma dispersion and therefore a different temporal pulse shape. Also, other lower order harmonics are increased, as shown in Figure 6b, which significantly increases the fitness compared to the use of an argon broadened spectrum for pulse shaping. The same is true for 30 mbar (Figure 6c), here phase matching prevents low order harmonics in case of argon which can be compensated in case of SF₆. For 40 mbar (Figure 6d) the absolute yield after optimization is similar for both gases, but the spectral distribution is different. In case of SF₆ lower order harmonics are more pronounced.

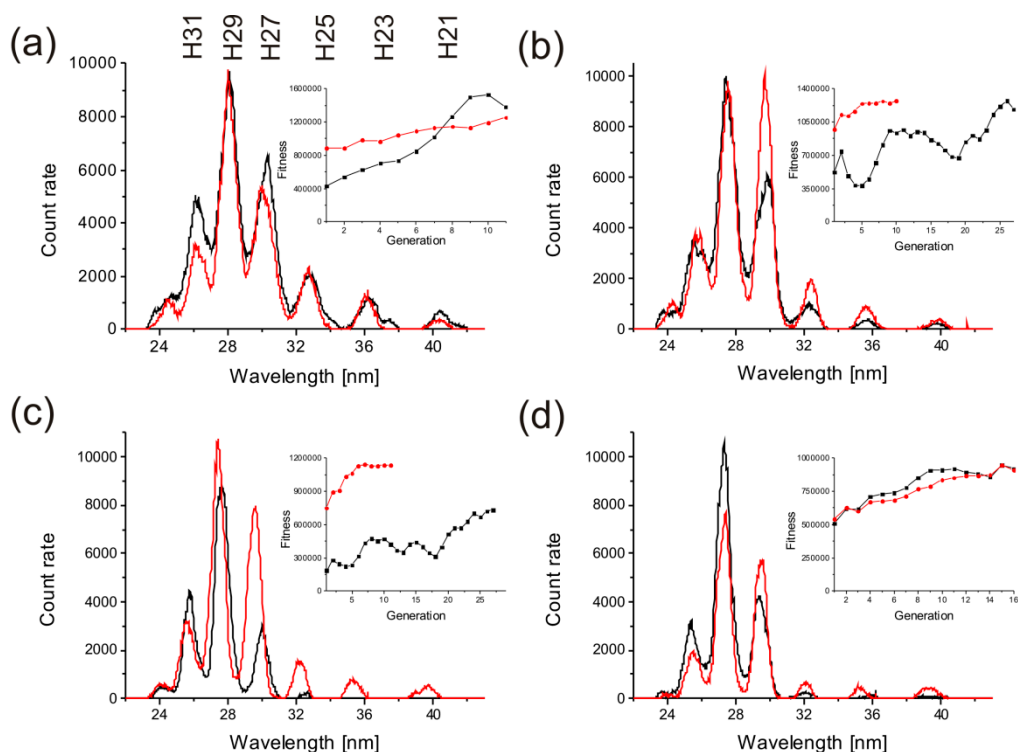


Figure 6. Optimized high-harmonic spectra from an argon-filled HCF are shown for temporally shaped pulses after spectral broadening in argon (black curve) and SF₆ (red curve). The optimization was performed to achieve the maximum yield between 23 and 43 nm and the fitness of the fittest individual of each generation is shown in the inset. The optimizations were performed at (a) 10 mbar; (b) 20 mbar; (c) 30 mbar and (d) 40 mbar argon backing pressure in the high-harmonic generation (HHG)-HCF.

To conclude, for higher gas pressures the XUV spectra of the in SF₆ broadened and subsequently shaped pulse show a larger amount of lower order harmonics, which increases the total bandwidth of the XUV spectrum. In a certain parameter range, the XUV yield can be doubled compared to the use of argon for spectral broadening.

3.2. Selection of Single Harmonics

The optimization experiments for a single harmonic are shown in Figure 7. The applied optimization strategy was as follows: the signal in a certain spectral region (marked with a colored bar in Figure 7a,c) has been maximized, after normalization to the signal summed up over the full displayed spectral region. So the fitness is maximized if the signal is relatively enhanced in a defined spectral region also at the expense of a lower absolute signal level. Note that the described optimization of a fraction of the signal is not appropriate for the realization of a high-flux source, requiring the optimization of the fractional signal and the total signal. As we are interested in comparison of different broadening media, we limit ourselves here to relative optimization of selected spectral features.

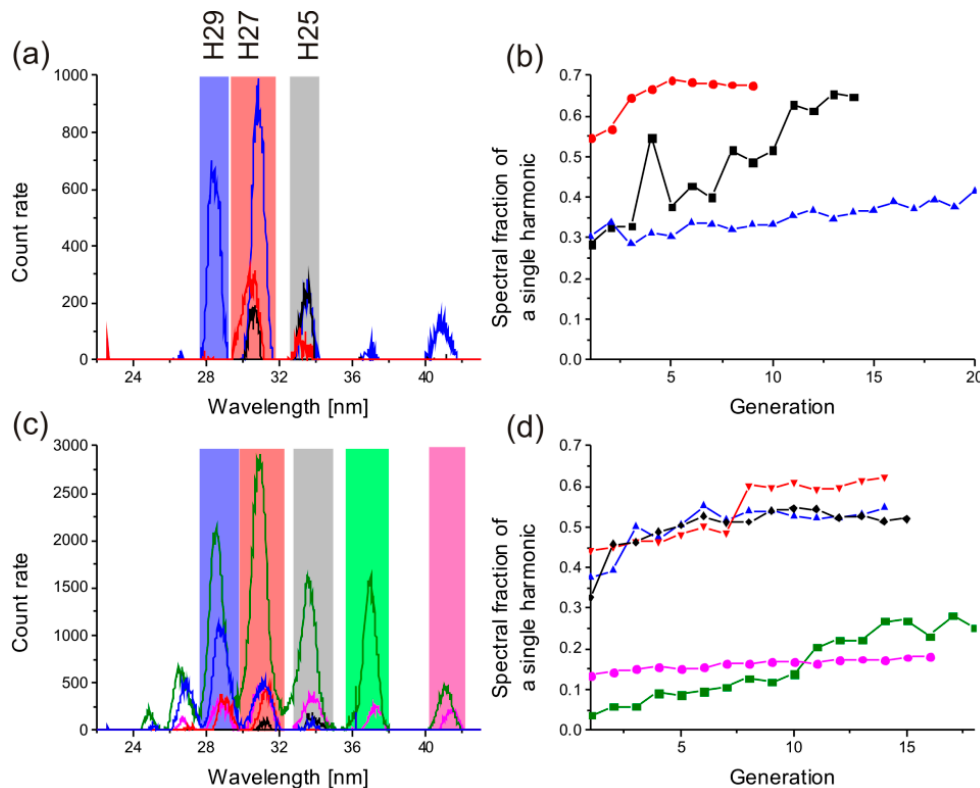


Figure 7. Optimization of single harmonics for (a) argon broadened and (c) SF₆ broadened shaped pulses. The colored areas show the chosen spectral area for the optimization and the respective optimization result is shown as a line plot. The accompanying development of the fitness is shown in (b) and (d) in the same color as the optimized spectra. In case of using SF₆ the spectral fraction of 25th to 29th harmonic can be optimized over 50%.

Using argon for spectral broadening the results for selective optimization of three different spectral regions are shown in Figure 7a, and in Figure 7b we depict the evolution of the fitness. The most

remarkable observations are: (i) for selection of the 29th harmonic (blue marked range) the fitness only slightly increases and the low energy harmonics still substantially contribute to the observed spectrum; (ii) for the 27th harmonic (red marked range) the spectral fraction can be increased up to 65% of the spectrum. However, the spectral selection is achieved at the cost of a reduced total count rate; (iii) Optimization for the 25th harmonic (black) shows an increase of the spectral fraction of the harmonic by a factor of 2. The absolute yield of the 25th harmonic is very similar to that of the optimization for the 29th harmonic but lower and higher orders of harmonics are suppressed.

Using SF₆ for spectral broadening only two different evolutions of the optimization can be observed as shown in Figure 7c,d. For high energy harmonics (blue, red and black marked regions) a single harmonic can be increased above 50% of the spectrum. For lower order harmonics (green and purple marked regions) even after optimization the spectrum contains all harmonics and the spectral fraction of a single harmonic is below 30%. This different behavior using SF₆ instead of argon for spectral broadening can be attributed to a slightly changed phase profile due to the SRS contribution, *i.e.*, will enhance the dynamic range for the phase only pulse-shaping, because spectral components, which are not needed for putting together the ideal pulse in time domain, can be suppressed by stretching them in the time domain. On the other hand, the role of the missing spectral parts in case of argon can be hardly enhanced by a phase shaper.

Summing up, the selection of single harmonics works best for the 27th harmonic (red area in Figure 7a,c) independent of the medium for spectral broadening. In both cases this harmonic achieved the highest spectral fraction (above 60%). Using SF₆ for spectral broadening the spectral window for selective optimization is wider and allows us to enhance also 29th and 25th harmonic substantially and the corresponding development of the fitness is very similar.

4. Conclusions and Outlook

In conclusion, our experiments showed that it can be beneficial to change the typically used noble gas in an HCF setup to a molecular gas in case of performing pulse-shaping experiments to generate high harmonics. Using temporally shaped pulses and an HCF for HHG the XUV yield could be doubled and the spectral window for selective optimization of a single harmonic could be increased when using SF₆ for spectral broadening. Furthermore, it was shown that the characteristic of the XUV spectrum can be easily influenced by simply changing the gas which is used for spectral broadening without any further change of a single optical element. Thus, nonlinear fiber optics with molecular media offer large potential in ultrafast science. This can be of great interest when building up XUV beamlines for spectroscopy. Since using an HCF for spectral broadening is a standard technique in ultrafast science and nowadays a large variation of pulse-shaping devices becomes increasingly common to be implemented in laser systems, the general idea of switching to a molecular gas can be easily realized and offers, as in case of HHG, a lot of potential.

Tailored harmonic spectra are of immediate interest and importance for the field of stationary or time-resolved spectroscopy in the XUV and soft-X-ray regions [27]. A number of applications have demonstrated the use of this laboratory-scale light source for probing matter properties in spectral and temporal domain with XUV photon energies and femtosecond time resolution, *e.g.*, XUV scanning microscopy at 13 nm [28] or time-resolved photoemission spectroscopy of surface chemistry [29].

The possibility to shape high harmonics greatly extends the field of applications and broadens the level of information retrieved from such measurements. A lot of applications originally performed at synchrotrons become also available for tabletop HHG sources, e.g., studying absorptions edges of transitions metals [30,31]. This is also true for XUV imaging demanding for monochromatic illumination. This is usually achieved using spectral filtering when using an HHG spectrum as a source and obviously selection of a single harmonic by pulse-shaping can be advantageous compared to afterwards removal of unwanted wavelengths by XUV multilayer optics [32]. The mentioned applications may all be of benefit when a molecular gas is used for pulse-shaping.

Acknowledgments

The authors gratefully acknowledge support from the European Regional Development Fund (EFRE) and the state of Thuringia (TMBWK). M.Z. acknowledges support from the Humboldt Foundation.

Author Contributions

The experimental data were collected by A.H. and M.Z. All authors analyzed the data and contributed to the completion of the manuscript.

Conflicts of Interest

The authors declare no conflict of interest. The founding sponsors had no role in the design of the study; in the collection, analyses, or interpretation of data; in the writing of the manuscript, and in the decision to publish the results.

References

1. Krausz, F.; Ivanov, M. Attosecond physics. *Rev. Mod. Phys.* **2009**, *81*, 163–234.
2. Itatani, J.; Levesque, J.; Zeidler, D.; Niikura, H.; Pepin, H.; Kieffer, J.C.; Corkum, P.B.; Villeneuve, D.M. Tomographic imaging of molecular orbitals. *Nature* **2004**, *432*, 867–871.
3. Winterfeldt, C.; Spielmann, C.; Gerber, G. Colloquium: Optimal control of high-harmonic generation. *Rev. Mod. Phys.* **2008**, *80*, 117–140.
4. Pfeifer, T.; Spitzepf, R.; Walter, D.; Winterfeldt, C.; Dimler, F.; Gerber, G.; Spielmann, C. Towards optimal control with shaped soft-X-ray light. *Opt. Express* **2007**, *15*, 3409–3416.
5. Wang, X.; Jin, C.; Lin, C.D. Coherent control of high-harmonic generation using waveform-synthesized chirped laser fields. *Phys. Rev. A* **2014**, doi:10.1103/PhysRevA.90.023416.
6. Zürch, M.; Rothhardt, J.; Hädrich, S.; Demmler, S.; Krebs, M.; Limpert, J.; Tünnermann, A.; Guggenmos, A.; Kleineberg, U.; Spielmann, C. Real-time and sub-wavelength ultrafast coherent diffraction imaging in the extreme ultraviolet. *Sci. Rep.* **2014**, doi:10.1038/srep07356.
7. Zürch, M.; Foertsch, S.; Matzas, M.; Pachmann, K.; Kuth, R.; Spielmann, C. Cancer cell classification with coherent diffraction imaging using an extreme ultraviolet radiation source. *JMIOBU* **2014**, doi:10.1117/1.JMI.1.3.031008.

8. Spielmann, C.; Burnett, N.H.; Sartania, S.; Koppitsch, R.; Schnurer, M.; Kan, C.; Lenzner, M.; Wobrauscheck, P.; Krausz, F. Generation of coherent X-rays in the water window using 5-femtosecond laser pulses. *Science* **1997**, *278*, 661–664.
9. Serrat, C.; Roca, D.; Seres, J. Coherent amplification of attosecond light pulses in the water-window spectral region. *Opt. Express* **2015**, *23*, 4867–4872.
10. Nisoli, M.; de Silvestri, S.; Svelto, O.; Szipocs, R.; Ferencz, K.; Spielmann, C.; Sartania, S.; Krausz, F. Compression of high-energy laser pulses below 5 fs. *Opt. Lett.* **1997**, *22*, 522–524.
11. Russell, P.S.; Holzer, P.; Chang, W.; Abdolvand, A.; Travers, J.C. Hollow-core photonic crystal fibres for gas-based nonlinear optics. *Nat. Photonics* **2014**, *8*, 278–286.
12. Okell, W.A.; Witting, T.; Fabris, D.; Austin, D.; Bocoum, M.; Frank, F.; Ricci, A.; Jullien, A.; Walke, D.; Marangos, J.P.; *et al.* Carrier-envelope phase stability of hollow fibers used for high-energy few-cycle pulse generation. *Opt. Lett.* **2013**, *38*, 3918–3921.
13. Zhavoronkov, N.; Korn, G. Generation of single intense short optical pulses by ultrafast molecular phase modulation. *Phys. Rev. Lett.* **2002**, doi:10.1103/PhysRevLett.88.203901.
14. Turner, F.C.; Strickland, D. Anti-stokes enhancement of multifrequency raman generation in a hollow fiber. *Opt. Lett.* **2008**, *33*, 405–407.
15. Turner, F.C.; Trottier, A.; Strickland, D.; Losev, L.L. Transient multi-frequency raman generation in SF₆. *Opt. Commun.* **2007**, *270*, 419–423.
16. Zhavoronkov, N. Efficient spectral conversion and temporal compression of femtosecond pulses in SF₆. *Opt. Lett.* **2011**, *36*, 529–531.
17. Landgraf, B.; Hoffmann, A.; Kartashov, D.; Gärtner, F.; Samsonova, Z.; Polynkin, P.; Jacoby, J.; Kühl, T.; Spielmann, C. Generation of multi-millijoule red-shifted pulses for seeding stimulated raman backscattering amplifiers. *Opt. Express* **2015**, *23*, 7400–7406.
18. Hoffmann, A.; Zürch, M.; Gräfe, M.; Spielmann, C. Spectral broadening and compression of sub-millijoule laser pulses in hollow-core fibers filled with sulfur hexafluoride. *Opt. Express* **2014**, *22*, 12038–12045.
19. Pfeifer, T.; Walter, D.; Winterfeldt, C.; Spielmann, C.; Gerber, G. Controlling the spectral shape of coherent soft X-rays. *Appl. Phys. B* **2005**, *80*, 277–280.
20. Nibbering, E.T.J.; Grillon, G.; Franco, M.A.; Prade, B.S.; Mysyrowicz, A. Determination of the inertial contribution to the nonlinear refractive index of air, N₂, and O₂ by use of unfocused high-intensity femtosecond laser pulses. *J. Opt. Soc. Am. B* **1997**, *14*, 650–660.
21. Carman, R.L.; Mack, M.E. Experimental investigation of transient stimulated raman scattering in a linearly dispersionless medium. *Phys. Rev. A* **1972**, doi:10.1103/PhysRevA.5.341.
22. Everall, N.J.; Partanen, J.P.; Barr, J.R.M.; Shaw, M.J. Threshold measurements of stimulated raman scattering in gases using picosecond krf laser pulses. *Opt. Commun.* **1987**, *64*, 393–397.
23. Rundquist, A.; Durfee, C.G.; Chang, Z.H.; Herne, C.; Backus, S.; Murnane, M.M.; Kapteyn, H.C. Phase-matched generation of coherent soft X-rays. *Science* **1998**, *280*, 1412–1415.
24. Holgado, W.; Alonso, B.; Roman, J.S.; Sola, I.J. Temporal and spectral structure of the infrared pulse during the high order harmonic generation. *Opt. Express* **2014**, *22*, 10191–10201.
25. Anderson, P.N.; Horak, P.; Frey, J.G.; Brocklesby, W.S. High-energy laser-pulse self-compression in short gas-filled fibers. *Phys. Rev. A* **2014**, doi:10.1103/PhysRevA.89.013819.

26. Serrat, C. Broadband spectral amplitude control in high-order harmonic generation. *Appl. Sci.* **2012**, *2*, 816–830.
27. Haight, R.; Seidler, P.F. High-resolution atomic core-level spectroscopy with laser harmonics. *Appl. Phys. Lett.* **1994**, *65*, 517–519.
28. Fruke, R.; Kutzner, J.; Witting, T.; Zacharias, H.; Wilhein, T. EuV scanning transmission microscope operating with high-harmonic and laser plasma radiation. *Europhys. Lett.* **2005**, *72*, 915–921.
29. Haarlammert, T.; Zacharias, H. Application of high harmonic radiation in surface science. *Curr. Opin. Solid State Mater. Sci.* **2009**, *13*, 13–27.
30. Berlasso, R.; Dallera, C.; Borgatti, F.; Vozzi, C.; Sansone, G.; Stagira, S.; Nisoli, M.; Ghiringhelli, G.; Villoresi, P.; Poletto, L.; *et al.* High-order laser harmonics and synchrotron study of transition metals $M_{2,3}$ edges. *Phys. Rev. B* **2006**, doi:10.1103/PhysRevB.73.115101.
31. Loh, Z.H.; Khalil, M.; Correa, R.E.; Leone, S.R. A tabletop femtosecond time-resolved soft X-ray transient absorption spectrometer. *Rev. Sci. Instrum.* **2008**, doi:10.1063/1.2947737.
32. Guggenmos, A.; Jobst, M.; Ossiander, M.; Radunz, S.; Riemsberger, J.; Schaffer, M.; Akil, A.; Jakubeit, C.; Bohm, P.; Noever, S.; *et al.* Chromium/scandium multilayer mirrors for isolated attosecond pulses at 145 eV. *Opt. Lett.* **2015**, *40*, 2846–2849.

© 2015 by the authors; licensee MDPI, Basel, Switzerland. This article is an open access article distributed under the terms and conditions of the Creative Commons Attribution license (<http://creativecommons.org/licenses/by/4.0/>).